



Biomineralization behavior of ternary mesoporous bioactive glasses stabilized through ethanol extraction process

Sudipta^a, Sarita Mishra^{b,c}, Sevi Murugavel^{a,*}

^a Department of Physics and Astrophysics, University of Delhi, Delhi, 110007, India

^b CSIR- Institute of Genomics and Integrative Biology, Mathura Road, New Delhi, 110025, India

^c Academy of Scientific and Innovative Research (AcSIR), Ghaziabad, 201002, India



ARTICLE INFO

Keywords:

Mesoporous bioactive glass
Apatite phase
High surface area
Biomineralization

ABSTRACT

The development of bioactive implantable materials with multi-functional properties like tissue regeneration, tumor annihilation, anti-bacterial growth and angiogenesis advancement is of great importance. In this context, mesoporous bioactive glasses (MBGs) are gaining tremendous interest in designing the next generation of biomaterials for the bone defect treatment. In this work, ternary $\text{SiO}_2\text{-CaO-P}_2\text{O}_5$ MBGs have been synthesized by using the acid assisted sol-gel process. In contrast to the conventional process, we adopted an ethanol extraction process to remove surfactant, leading to superior textual properties and high silanol group density in resultant bioglass. Magic angle spinning nuclear magnetic resonance (MAS-NMR) technique has been used to elucidate the presence of different anionic species in the pristine glass samples and its variation with chemical compositions. The vibrational spectroscopy reveals the presence of high concentration of silanol group over the surface of pristine glass samples, which effectively accelerates the formation of hydroxyl carbonate apatite (HCA) layer. The MBG specimens show a good cell viability behavior without toxicity up to the concentration of $20 \mu\text{g ml}^{-1}$. In the present results, we observed that pore size along with surface area and silanol group density play an effective role in the growth of HCA layer.

1. Introduction

The bioactivity and biocompatibility of bioactive glasses (BGs) have directed them to be investigated for its use as an implant material in human body to repair and replace diseased or damaged bones [1,2]. The bone defects usually arise by many reasons, like through tumor removal, trauma, or cleft palates [3–5]. More commonly, biodegradable bioactive glasses classified under the third generation of biomaterials have ability to form bond with both soft and hard tissues and also exhibit the unique properties like osteoconduction, osteostimulation and osteoinduction [2,3]. Advantageously, BGs combined with mesoporous structure lead to the faster and controlled dissolution of ions from the sample and enhances the apatite formation. These materials react and dissolve in the physiological fluid and it can replace the damaged bone and tissue cells over a period of time. In addition, the third generation biomaterials are subjected to specific interaction with cell integrins and thereby cell-proliferation and differentiation. These mesostructured BGs are being expected to trigger genes that stimulate the regeneration of living tissues. Hence, they are highly indispensable in the fields of bone healing

process, dentistry, cell tissue interaction, proliferation and differentiation of the cells [2–4]. The subject of bioactive glass has been intensively studied over the last fifty years for the development of various types of BGs, including silicate, borate/borosilicate and phosphate-based bioactive glasses with improved properties [6–8]. More specifically, the glass systems like $\text{SiO}_2\text{-CaO}$ or $\text{SiO}_2\text{-CaO-P}_2\text{O}_5$ brings out significantly improved bioactivity compared with conventional 45S5 bioglass, making it an ideal component for bone regenerations.

It is well established that the mesoporous bioactive glasses combine the excellent textual parameters of ordered mesoporous matrices with the properties of conventional bioactive sol-gel glasses. Hence, MBGs become ideal for the bone tissue regeneration and drug delivery system [9]. The mesoporous structure is controlled by different parameters such as synthesis conditions, temperature, acidity, reactant ratios, gelation time, stabilization step and the type of surfactant used as a structure-directing agent [10,11]. Recently, the applications of MBGs have leaped a significant step forward by including controllable amount of different ions in the bioactive glass composition. More specifically, an ultimate aim is to impart other biological functions such as stimulation

* Corresponding author.

E-mail address: murug@physics.du.ac.in (S. Murugavel).

of osteogenesis, anti-bacterial activity and angiogenesis by means of the inclusion of metallic elements with therapeutic effect [12]. Different studies have been undertaken with incorporation of various therapeutic ions, including Ag^+ , Sr^{2+} , Cu^{2+} and Co^{2+} into MBGs and their release rate is related to the enhancement of several biological functions [13–17]. In addition, large surface area and accessible pore volume possessed by MBGs provide exceptional drug delivery ability that synergistically combined with the release of therapeutic ions and can be exploited to develop multifunctional materials. Another interesting aspect of silica-based mesoporous bioactive glass is that it contains high silanol group density on the surface, hence, it can easily be functionalized through a post grafting process to improve drug loading and controlled drug release ability [18,19].

Some of the recent investigations have focused on developing MBG particles characterized by their size ranging from ten to hundreds of nanometers having good surface bioreactivity. In this context, different strategies have been developed to synthesize MBGs with hierarchical textural properties which favor the easy dissolution of glass particles followed by the enhanced hydroxyapatite formation upon their immersion in simulated body fluid (SBF). Among the various approaches, introduction of supramolecular chemistry approach in the sol-gel route to obtain highly porous glass particle in mesoporous range is the newest approach. This method involves the use of polymeric surfactant as structure directing agent (SDA) and the evaporation induced self-assembly (EISA) process [20]. Typically, the EISA process includes the use of non-ionic triblock copolymer as SDA and its unique self-assembly characteristics, which allow us to achieve well-ordered mesoporous structures. The MBGs found to be more attractive now-a-days as they have an excellent bioactivity level due to their highly ordered mesoporous network structure and excellent textural characteristics [21–23]. Further, these mesoporous bioactive glasses exhibit the very prominent biocompatibility behavior and osteoconductivity property. After the EISA process, removal of the surfactant is mostly carried out by calcination process at high temperatures (above 500 °C) under atmospheric air [24]. The calcination-based methods provide a template free sample with consolidation of the silicate network and it is a simple and effective step for the removal of template string, i.e., non-ionic copolymer [25]. However, the calcination at high temperature follows the negative results, where structural shrinkage, aggregation of colloidal particles, partial disordering and a significant reduction in silanol groups on the glass surface have been observed [26]. An extraction-based method is an alternative method for removing surfactant using an organic solvent or a supercritical fluid. It is a low-temperature stabilization process by using a solvent [27,28]. Therefore, the glass particle stabilized through the ethanol extraction method possesses initial porous structure and high density of silanol (Si-OH groups), because no consolidation and shrinkage occur in this process. Typically, the solvent extraction process cannot produce the complete template free MBG sample with multiple repetitions [29]. Therefore, a two-step template removal process such as solvent extraction and calcination or microwave-assisted extraction has been adopted [30,31]. The Si-OH group, which remains after the template removal process, strongly enhances the hydroxyl carbonate apatite (HCA) formation and absorption capacities of sample. Therefore, MBGs containing the Si-OH groups are more prominent candidates for bone regeneration and drug delivery applications.

In the present work, we have reported the synthesis of mesoporous $\text{SiO}_2\text{-CaO-P}_2\text{O}_5$ glasses by a modified sol-gel route followed by the EISA process. In the final stage of synthesis, glass samples were stabilized through the two-step process which involves acid treatment followed by ethanol extraction process. The pristine MBGs are characterized by various analytical techniques to evaluate its structure, morphology and textural properties. Remarkably, the textural study reveals that the obtained MBGs possess an enhanced surface area and pore volume. MAS-NMR technique on the obtained glass samples shows the presence of various anionic species and its variation with chemical compositions. Subsequently, we have carried out an *in-vitro* bioactivity study on the

MBGs to ascertain the biomaterialization behavior. MBGs in this work do not follow the first three steps of Hench Mechanism (HM) due to high surface area and high density of silanol group as per the ICP-MS study and the variation of pH of simulated body fluid (SBF) solution with different soaking time intervals. The deposition of HCA layer on the surface of MBG samples has been determined through FTIR, FESEM and HR-TEM techniques. We have also discussed the effect of surface area and silanol group density which not only affect the biomaterialization behavior of MBGs but also the stability, growth and crystallization of HCA phase. Further, we made an effort to understand the other active factors such as pore size, concentration of Si-OH group and pH of SBF solution on the biomaterialization behavior of MBGs.

2. Experimental section

In this work, we have chosen the ternary $\text{SiO}_2\text{-CaO-P}_2\text{O}_5$ glass system with different chemical compositions, as listed in **Table S1** (See ESI). The glasses are prepared through an acid-assisted template sol-gel route followed by the evaporation-induced self-assembly (EISA) process. In the modified sol-gel synthesis method, the supramolecular chemistry of surfactant incorporated into a conventional sol-gel method for obtaining an ordered mesopore structure [20]. Generally, in sol-gel route, the metal alkoxides are used as precursors due to high solubility in ethanol and immiscibility of Si-O covalent bond (hydrophobic) with water follows a glass formation with rigid network. The given chemicals are used as precursors for the synthesis of MBGs: Tetraethyl orthosilicate [TEOS: $\text{Si}(\text{OC}_2\text{H}_5)_4$], reagent grade 98%, used as a precursor for SiO_2 , a structure-forming agent; Triethyl phosphate [TEP: $(\text{C}_2\text{H}_5\text{O})_3\text{PO}_4$], ≥ 99.8% used for P_2O_5 ; Calcium acetate hydrate [$\text{CaAc:Ca}(\text{CH}_3\text{COO})_2 \cdot x\text{H}_2\text{O}$], reagent grade ≥ 99%, is used for CaO a modifier, Non-ionic amphiphilic triblock co-polymer [Pluronic P123: $\text{EO}_{20}\text{PO}_{70}\text{EO}_{20}$], used as structure-directing agent (SDA). In the chemical formula of P123, EO stands for poly (ethylene oxide) a hydrophilic part, while PO for poly (propylene oxide) a hydrophobic part. Acetic Acid [CH_3COOH] used as a catalyst for fast hydrolysis of TEOS and TEP to get homogeneous sol and Ethanol [Eth: $\text{C}_2\text{H}_5\text{OH}$] as a solvent for TEOS. Ethanol does not play a simple role in reaction while it has an active part in the synthesis process. The organic solvent ethanol provides an appropriate environment for the self-organization of P123 molecules into the micelles. These micelles are effective for the formation of ordered mesoporous structure through the link-up of hydrolyzed silica with the hydrophilic part of micelles [11]. Additionally, the acetic acid also avoids the micelle aggregation and carbon contamination [32]. All precursors are purchased from the Sigma Aldrich and used without further purification. Deionized water has been used for the proper hydrolysis of TEOS and TEP.

For the synthesis of MBGs, the precursors TEOS, TEP, CaAc are taken with the desired molar ratio, which is designed according to the molar ratio of SiO_2 , CaO and P_2O_5 content given in the **Table S1** (See ESI). The sol-gel route involves transition of sol into the gel. In order to form the homogeneous sol, 1 g of P123 surfactant is dissolved in 15 g of ethanol and followed by the addition of all precursors one by one at an interval of one-hour, keeping the constant molar ratio of TEOS/TEP: Ethanol: 1:4, TEOS/TEP: Water: 1:4, the weight ratio of Acid: Water: 1:6. The admixture kept for stirring at ambient temperature until the sol becomes gel. The resulting gel is then placed into a vacuum oven to undergo the EISA process using Borosil Petri Dish. EISA process involves the aging of gel for three days at 40 °C and then dried at 60 °C for 24 hrs to remove excess solvents, catalysts and by-products, consequently, a rigid interconnected pore network is obtained.

In order to have the desired porous structure the final stage of sol-gel process is crucial, i.e., template removal. In this step, tailoring of the textural properties takes place, including surface area, pore size, pore volume, pore ordering and density of silanol groups. For removing the triblock copolymer template to get mesoporous bioactive glass, we have adopted the two-step method. The first step involves the acid treatment process; 20 mg of the resultant sample is mixed with 1 ml of sulphuric

acid (48 wt%) for 3 hours at 65 °C by allowing the sample to remain in the amorphous state with continuous monitoring during each step. In this step, only PO chains of the surfactants decompose and H₂SO₄ is helpful in the oxidation of polymer and the resulting admixture is washed with water until eluent becomes neutral [33]. Subsequently, we used the ethanol extraction process for the complete removal of P123 from the resulting product.

The ethanol washing has been carried out by refluxing the powder samples in ethanol medium stirring it overnight. After continuous stirring, the samples are washed repeatedly four times with ethanol using a centrifuge at 4000 rpm for 30 min. The ethanol extraction stabilization process has an advantage over the conventional calcination method with its low-temperature process. The mesoporous materials stabilized through the ethanol extraction method have high density of silanol group, high specific surface area and narrow pore size distribution without significantly shrinking of pores in the glass network [25]. Along with the above advantages, this method cannot completely remove the template in the resulting final products [29].

3. Result and Discussion

In Fig. 1, we illustrate the powder HR-XRD patterns of all pristine samples (82S, 70S and 58S; the given nomenclature is based on SiO₂ content in mol %). The obtained diffraction patterns of as-synthesized samples show a broad hump between 15 to 35°, which is characteristic nature of the silicate-based glasses. Thus, from HR-XRD results we confirmed that all three samples possess the amorphous structure and don't have any crystalline phases. In Figure S1 (See ESI), we show the TGA thermograms for 82S-BA, 82S-AA and 82S-AE, which are termed as 82S before acid (BA) treatment, 82S after acid (AA) treatment and 82S after ethanol (AE) washing process. The 82S-AA and 82S-AE glass powder thermograms are closely identical with a slight difference in weight loss at around 100 °C. The initial endothermic process in 82S-AA and 82S-AE is attributed to the loss of physically absorbed water and the significant share of traces retained in the pores during the washing process. The weight loss at 250–380 °C for 82S-AA is attributed to the loss of P123 that remained in the pores. The slight mass loss observed in both 82S-AA and 82S-AE is attributed to the structural densification. In the thermogram of 82S-BA, the overall weight loss at temperature 150–650 °C is attributed mostly to P123 decomposition [34]. The decomposed amount of P123 is approximately less than 1% for 82S-AE, 4% for 82S-AA and 51% for 82S-BA. These results indicate that ethanol extraction step provides better resultant product than the other methods of extraction. Hence, it is evident from the TGA thermogram that there is hardly any impurity to be volatilized after stabilization through ethanol

washing process and the obtained bioactive glass samples are almost free from P123.

3.1. FTIR Spectroscopy study

The FTIR spectroscopy technique is sensitive to the determination of local structure, different vibrational modes in silicate glasses and the presence of any trace amount of impurities. In Fig. 2, we represent the Fourier Transform Infrared (FTIR) spectra of all three pristine samples (82S, 70S and 58S) after stabilized through ethanol extraction. FTIR spectrum in the present study shows characteristic vibrational bands of silica-based bioactive glasses. The band located at 475 cm⁻¹ is assigned to the bending motion of bridging oxygen atoms of Si-O-Si group, i.e., vibrational motion of oxygen perpendicular to the Si-O-Si plane. The vibrational band at 800 cm⁻¹ is attributed to the symmetric stretching motion of oxygen atom of Si-O-Si bridging group. The vibrational band at 966 cm⁻¹ corresponds to the Si-O stretching vibration of Q_{Si}² (Si-O-2NBO) unit [35]. Moreover, an intense band at 1092 cm⁻¹ in the high-frequency region is attributed to internal asymmetric stretching mode of Si-O-Si group involving mainly the motion of oxygen atom in Q_{Si}⁴ species [36]. Furthermore, the absence of a low-intensity band at ~1450 cm⁻¹ corresponding to the deformation modes of CH₂ and CH₃ groups confirmed the absence of template residuals [25]. The vibrational band at 583 cm⁻¹ is assigned to PO₄³⁻ unit (O-P-O, O=P-O type of bonds).

Interestingly, FTIR spectra reveal the presence of different types of hydroxyl group (OH) in the pristine samples; the vibrational band at 3455 cm⁻¹ is assigned to silanol groups and the band centered at 1635 cm⁻¹ is attributed to the presence of OH group due to water absorption [37]. The intensity of this band increases with the addition of CaO content, which creates a greater number of NBO (non-bridging oxygen).

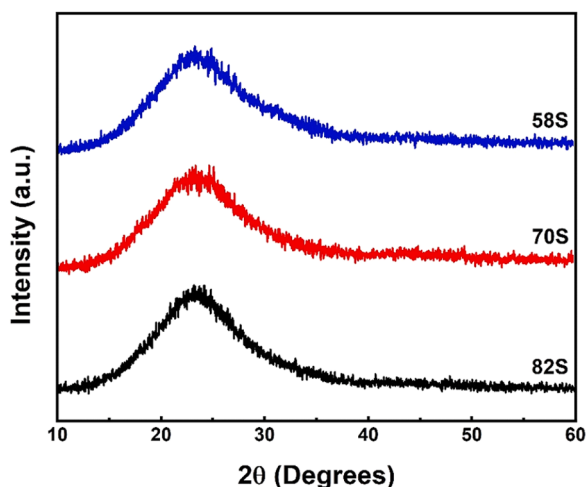


Fig. 1. HR-XRD patterns of mesoporous bioactive glasses in the pristine form.

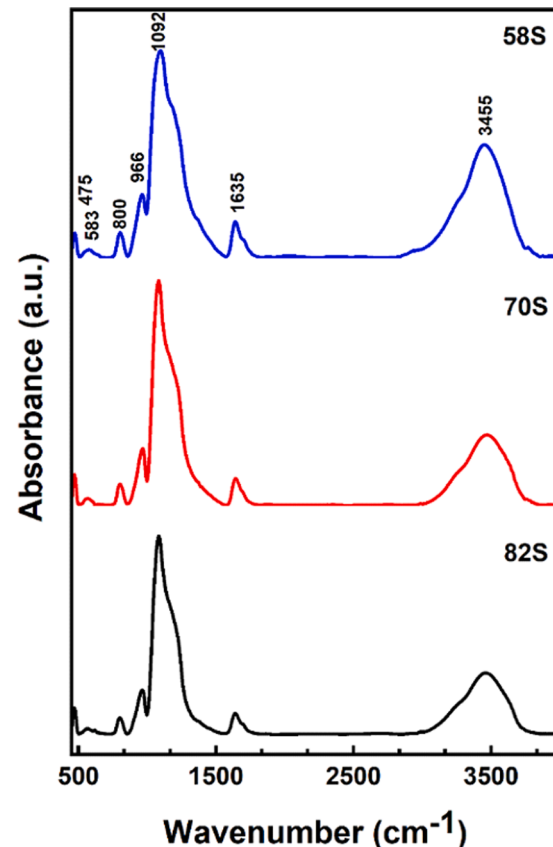


Fig. 2. FTIR spectra of 82S, 70S and 58S MBGs after stabilized through ethanol washing.

Remarkably, during the ethanol extraction stabilization step high density of silanol groups are retained. The silanol group is crucial for the formation of hydroxyapatite, drug loading and release properties of the MBGs [11]. The band at around 1092 cm^{-1} becomes broader with P_2O_5 content, which suggests that different PO_4^{3-} vibrational modes largely participate in 58S MBG by silicate bands. The band corresponding to Q_{Si}^2 (Si-O-2NBO) species is well defined for all three samples, which predict the modifying behavior of CaO content in silicate-based bioactive glasses. The P_2O_5 content in silicate bioactive glasses acts as both modifier and network former and it depends on the mol % of P_2O_5 component [38]. Hence, the nature of P_2O_5 in silicate glasses has control on the structure consequently on textural properties. In silicate glasses, the alkaline-earth metal oxide (CaO) acts as a network modifier, conventionally, their presence reduces the degree of connectivity in the network through the replacement of bridging oxygen by NBO species (Si-O-NBO) as a result of breaking of Si-O-Si bonds between the tetrahedral units of SiO_4 [39]. The presence of Si-O-NBO groups in bioactive glass network supports the exchange of alkaline-earth element (Ca^{2+}) with H^+ or H_3O^+ from surrounding solution [1]. Further, it minimizes the concentration of NBOs required to have an efficient ion exchange, dissolution of silica network and formation of a SiO_2 rich layer on the surface of biomaterials [35].

In order to quantify the structural behavior of P_2O_5 content in all as-prepared MBGs, by a careful inspection of spectral shape, we have carried out deconvolution procedure by using Gaussian fitting in the frequency range from 860 to 1575 cm^{-1} on all three glass samples. The individual band assignments are based on earlier reported literatures on alkali and alkaline-earth modified silicate and phosphate glasses [35, 40-44]. The band position and relative amount of different vibrational modes have been estimated from the deconvoluted Gaussian peaks as shown in Figure S2 (See ESI). The position of Gaussian lines, fitted Gaussian parameters, peak assignment associated with different mode of vibrations are listed in Table S2 (See ESI). The deconvoluted data successfully explains the characteristic vibrations of different molecular groups P=O , P-O^- , PO_4^{3-} , P-O-P stretching and ionic character of phosphate group with P_2O_5 content in terms of vibrational intensity and centered position of vibrational peaks. The vibrational peak within $1000\text{-}1200\text{ cm}^{-1}$ range is assigned to asymmetric stretching vibrations of Si-O-Si in Q_{Si}^4 species [40]. The deconvolution procedure provides relative proportion of different bond in the phosphate groups.

It has been observed that the relative proportion of Q_{Si}^4 in Si-O-Si species decreases significantly with increasing the modifier alkaline oxide (CaO) concentration. The shifting in the peak position within $1000\text{-}1200\text{ cm}^{-1}$ range towards higher wavenumber side occurs due to the formation of Si-O-P chain by the occupation of P^{5+} at Si^{4+} lattice site [45]. The link-up of phosphorous, shifts the peak position towards right-hand side because phosphorous has higher electronegativity ($P_{\text{en}} = 2.19$) than silicon ($Si_{\text{en}} = 1.9$). The vibrational bands at 968 , 967 and 964 cm^{-1} for 82S, 70S and 58S samples, respectively, correspond to the Si-O stretching vibration of Q_{Si}^2 (Si-O-2NBO) unit [35], which shows a significant variation among the three glass compositions. The intensity of ν_s (Si-O-2NBO) vibrational band increases with the increase in CaO content and confirmed the formation of non-bridging oxygen. It has been reported that the asymmetric stretching vibration of P-O-P bridging oxygen lies in the region $888\text{-}922\text{ cm}^{-1}$ [41]. In the present work, bands attributed to ν_{as} (P-O-P) vibrational mode are observed at 935 , 930 and 922 cm^{-1} for 82S, 70S and 58S samples. It has been reported that the proportion of ν_{as} (P-O-P) vibrational mode increases with P_2O_5 concentration which may be due to the transformation of orthophosphate to pyrophosphate phase [42]. But in the present case, the contribution of ν_{as} (P-O-P) vibrational mode is less for 70S sample and higher for the 82S sample. The vibrational bands within the $980\text{-}1050\text{ cm}^{-1}$ and $1140\text{-}1180\text{ cm}^{-1}$ range corresponds to symmetric and anti-symmetric stretching mode of vibration (PO_3) for non-bridging oxygen (P-O^- group). The intensity of ν_s (P-O^-) increases with P_2O_5

concentration while decreases for ν_{as} (P-O^-) mode. Furthermore, the vibrational bands within $1200\text{-}1250\text{ cm}^{-1}$ range, i.e., 1212 , 1213 and 1211 cm^{-1} for 82S, 70S and 58S samples, respectively, are ascribed to the P=O stretching mode of vibration exists in the orthophosphate units. Additionally, the vibrational bands at 1261 , 1290 and 1325 cm^{-1} for 82S, 70S and 58S samples, respectively, are attributed to asymmetric stretching vibrations of O-P-O bonds. Thus, it is observed from the above discussion that the intensity of all peaks of phosphate group except the peak corresponds to ν_{as} (P-O^-) increases with P_2O_5 concentration. Further, it is clear that the modifier and network former behavior of P_2O_5 depending on its concentration are supported by the ^{31}P MAS-NMR results. Thus, P_2O_5 content plays an important role in the formation of different anionic species in all samples. It becomes crucial for CaP growth and the determination of textural properties of as-synthesized MBGs. In order to elucidate and quantify the various anionic species in these glasses, we have carried out the MAS-NMR technique.

3.2. MAS-NMR spectroscopy

In Fig. 3, we illustrate the ^{29}Si MAS-NMR deconvoluted spectra by using Gaussian fitting method with three components for 82S and 70S and four components for 58S sample. However, the raw spectra represent peaks corresponding to the different anionic species i.e., Q_{Si}^4 , Q_{Si}^3 , Q_{Si}^2

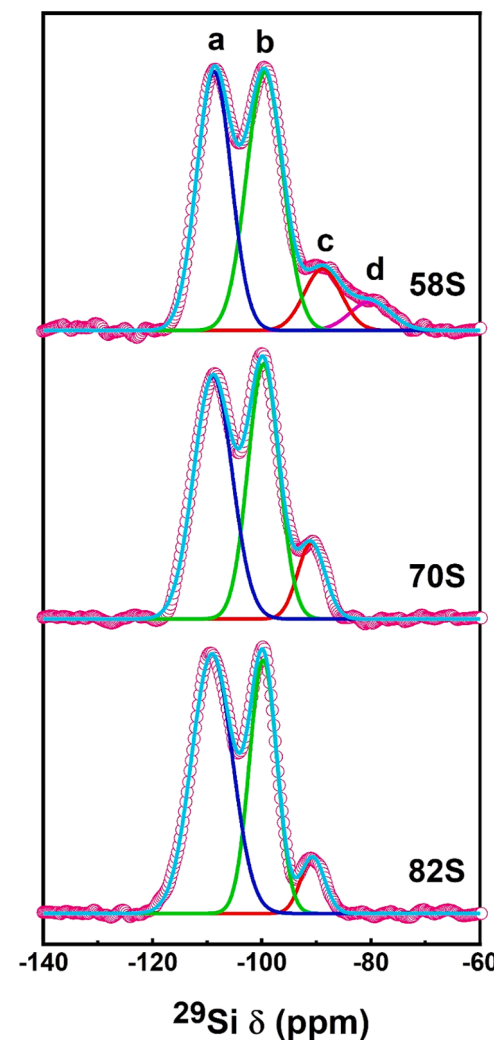


Fig. 3. ^{29}Si MAS-NMR spectra for pristine MBG samples after deconvolution into various Q-species for silica. (Open circle represents the raw spectra and solid line represents deconvoluted spectra)

and $Q_{Si}^2(Ca)$ present in 58S sample. The deconvolution has been carried out to compare the local structure of all three as-synthesized mesoporous bioactive glasses and to understand the role of CaO in local structure of all samples. The assigned chemical shift values to different anionic Q_{Si}^n species are based on the earlier investigations on silicate glasses consisting of alkali/alkaline earth metal ions [46–48]. The intense bands centered around -109 ppm and -99 ppm correspond to Q_{Si}^4 unit of the silicate network and Q_{Si}^3 species, respectively. The Q_{Si}^2 and $Q_{Si}^2(Ca)$ species are assigned to the chemical shift around -90 ppm and -80 ppm respectively and these bands represent the role of Ca in depolymerization of silica network [47]. From the deconvolution of NMR spectra, we provide the relative abundance (in area percentage) of extracted Q_{Si}^n species with corresponding chemical shift values in Table 1. Here, the network connectivity (NC) for silica has also been calculated from the deconvoluted peak area of ^{29}Si MAS-NMR spectrum and is given as:

$$NC_{Si} = 4 \times f(Q^4) + 3 \times f(Q^3) + 2 \times f(Q^2) + 1 \times f(Q^1)$$

where $f(Q^n)$ values are the fractional contributions of corresponding signals to the total area in ^{29}Si MAS-NMR spectrum [47].

In Table 1, the contribution of Q_{Si}^3 and Q_{Si}^2 species in the samples increases with an increase in concentration of CaO while it is reverse in order for the network connectivity, which shows the effect of modifier CaO on three-dimensional silicate network. The presence of $Si(OSi)_3OH$ and $Si(SiO)_2(OH)_2$ structural species on the surface of MBGs are confirmed by the ^{29}Si MAS-NMR spectra [47,49,50]. In Fig. 3 the ^{29}Si MAS-NMR spectrum of 58S specimen reveals the additional chemical shift at -80.06 ppm corresponding to $Q_{Si}^2(Ca)$ pointing out that the surface of 58S sample contains higher amount of Ca^{2+} ions than inner part [47]. Additionally, we also have acquired MAS-NMR spectra for the phosphate anionic species and studied the role of P_2O_5 in silicate network structure. In Fig. 4, we represent the deconvoluted ^{31}P MAS-NMR spectra fitted with Gaussian lines of pristine 82S, 70S and 58S MBGs and the extracted relative abundance of different species listed in Table 2. For 82S sample, three resonances at 0.97, -0.01 and -1.1 ppm are assigned as Brushite (dicalcium phosphate dihydrate, $CaHPO_4 \cdot 2H_2O$), calcium orthophosphate phase (Q_P^0) and Monetite (dicalcium phosphate dehydrate, $CaHPO_4$), respectively. The Brushite phase of calcium phosphate occurs due to large amounts of silanol and molecular water content [51–53]. In case of 70S sample, the resonance bands dominated at 0.76, -0.12 and -1.14 ppm are attributed to Brushite, calcium orthophosphate (Q_P^0) species and Monetite, respectively. The proportion of Brushite in 70S sample was higher than 82S and 58S samples and shows high percentage of silanol group on the surface of 70S sample, which has high surface area compared to 82S and 58S samples. Interestingly, the 58S glass sample exhibits the four resonance bands at 1.17, 0.05, -1.14 and -2.76 ppm, corresponding to Brushite, calcium orthophosphate (Q_P^0), Monetite and pyrophosphate (Q_P^1) respectively. The presence of pyrophosphate (Q_P^1) unit in 58S MBG confirmed P-O-Si bonding, which shows the network former behavior of phosphorus [54]. Thus, from ^{31}P MAS-NMR results, the network forming behavior of P_2O_5 becomes visible with increment in its concentration i.e., for 6 mol % of P_2O_5 . While in the case of 82S and 70S MBGs the P_2O_5 component completely behave as the network modifier. Therefore, from

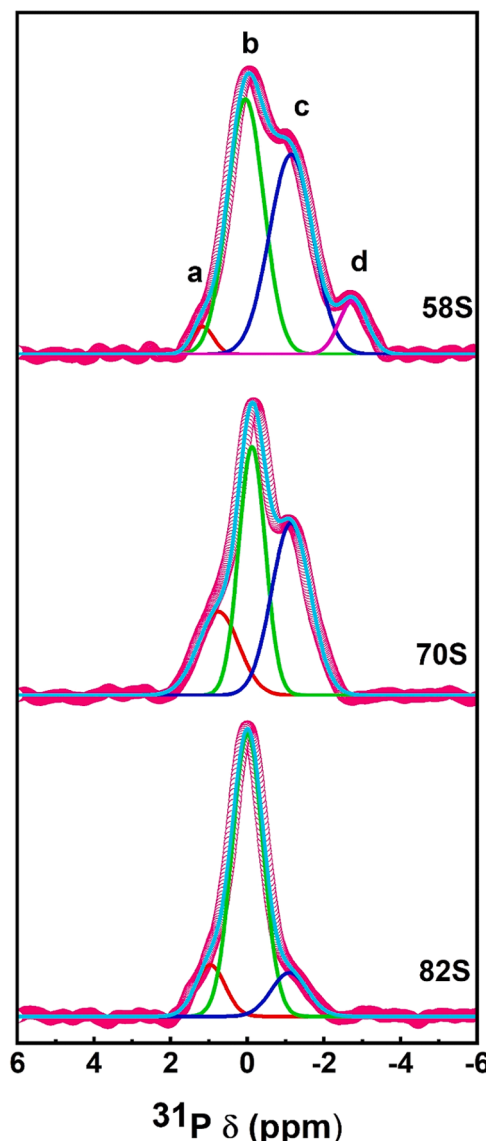


Fig. 4. ^{31}P MAS-NMR spectra for pristine MBG samples after deconvolution into varies Q-species for phosphate. (Open circle represents the obtained spectra and solid line represents deconvoluted spectra)

^{31}P MAS-NMR and BET results we concluded that the P_2O_5 effectively controls structural, Si-OH group density and textural properties of as-synthesized samples. As the network forming behavior of P_2O_5 becomes prominent, the pore size increases with reduction in the surface area, which can be seen in the BET results discussed in the following section.

3.3. Nitrogen adsorption-desorption measurement

Nitrogen adsorption-desorption technique is an essential

Table 1

Relative populations (expressed as area percentage) of Q_{Si}^n species obtained after deconvolution of the ^{29}Si MAS-NMR spectra and network connectivity of silica network.

Sample	Q_{Si}^4 (a)		Q_{Si}^3 (b)		Q_{Si}^2 (c)		$Q_{Si}^2(Ca)$ (d)		NC _{Si}
	$\delta(ppm)$	Area (%)	$\delta(ppm)$	Area (%)	$\delta(ppm)$	Area (%)	$\delta(ppm)$	Area (%)	
82S	-109.12	55.89	-99.73	36.99	-90.67	7.10			3.49
70S	-108.95	48.20	-99.66	41.04	-90.92	10.76			3.37
58S	-108.76	40.96	-99.44	43.20	-88.84	10.40	-80.06	5.44	3.25

Table 2

Relative populations (expressed as percentages) of Q_p^n species obtained after deconvolution of the ^{31}P MAS-NMR spectra.

Sample	Brushite (a)	Q_p^0 (b)	Monetite (c)	Q_p^1 (d)
	δ (ppm)	Area (%)	δ (ppm)	Area (%)
82S	0.97	12.89	-0.01	73.73
70S	0.76	20.54	-0.12	39.42
58S	1.17	3.01	0.05	46.29

characterization technique to investigate the textural characteristics of porous materials. Therefore, we have carried out the N_2 adsorption-desorption measurement for all three pristine powdered glass samples. Fig. 5 shows the nitrogen adsorption-desorption isotherm obtained together with pore size distribution for all the pristine samples. An obtained pristine glass samples exhibit type IV isotherm curve with H2 type of hysteresis loop [55]. The type IV isotherm is the characteristic of mesoporous structure, whereas H2 hysteresis loop confirmed the ink bottle like pores in as-synthesized MBG samples. The hysteresis loop for all samples is obtained at a high relative pressure (P/P_0) due to capillary condensation [56]. A narrow pore size distribution from desorption branch of the isotherm using Barrett-Joyner-Halenda (BJH) model has been obtained and inserted in Fig. 5. The pore size distribution represents the relatively narrow range and monomodal type of distribution. Additionally, we have carried out the t-method of analysis on all pristine samples to confirm the absence of micropores (pore size $< 2 \text{ nm}$). The textural properties of all pristine glass samples have been obtained and summarized in Table 3. The specific surface area has been determined by the Brunauer-Emmett-Teller (BET) method. It is interesting to note that the sol-gel synthesized mesoporous bioactive glasses, which were stabilized through ethanol washing method yield the superior textural parameters.

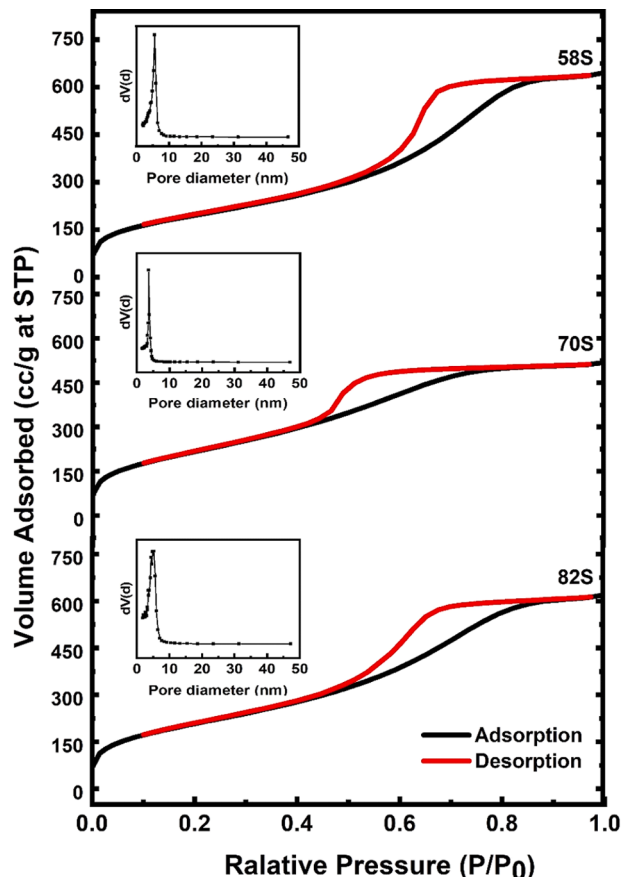


Fig. 5. N_2 -sorption isotherm (BET) and BJH pore size distribution (inset) of pristine mesoporous bioactive glass samples.

Table 3

Textural parameters obtained by N_2 -sorption measurement for the mesoporous bioactive glass samples.

MBG	Surface Area (m^2/g)	Pore Diameter (nm)	Pore Volume (cc/g)
82S	761.59 ± 1.51	4.21 ± 0.39	0.96 ± 0.19
70S	805.51 ± 1.25	3.33 ± 0.28	0.82 ± 0.24
58S	706.67 ± 1.69	4.67 ± 0.63	1.00 ± 0.24

Remarkably, we have found the highest surface area for all as-synthesized glass samples of similar chemical composition with respect to earlier reports in the literature [57]. We attribute the superior textural characteristics in the present work due to the ethanol washing procedure, which has low surface tension than water, exerts low drying stress and as a result, a high surface area is achieved. Additionally, it is known that several factors influence the textural parameters of glasses including porous silica-based bioactive glasses [37]. More commonly, the synthesis conditions (e.g., ratio of solvents to the surfactant content, temperature, gelation time and acidity/basicity of the catalyst, acid treatment step and stabilization method) are directly related to textural properties. Here, we have synthesized three different glass compositions with the similar synthesis condition and steps. In general, the surface area increases with silica content in silicate glasses [58]. It is interesting to note that surface area for 70S glass sample is higher than the other two compositions due to network modifying behavior of P_2O_5 [59]. The bioactive glasses stabilized through ethanol washing process possess superior textural properties than conventionally calcined bioactive glasses [57]. The high surface area and mesopore structure enhances the degradation of glass specimen during *in-vitro* bioactivity test and then the formation of HCA becomes easier with Si-OH group.

3.4. Morphological study

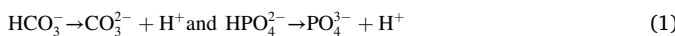
In Figure S3 (See ESI), we illustrate the typical FESEM micrographs of all the pristine samples. For the 82S sample, we illustrate the micrograph for two different magnifications at 1 kX and 100 kX in order to have microstructural differences with magnification. The FESEM images of all pristine samples at higher magnification retrieve the homogeneous surface for 82S, 70S and 58S glass samples. The surface morphology of pristine glass sample particles exhibits a porous texture. The micrograph of 82S and 58S represents the uniform distribution of considerable spherical glass particles as compared to 70S composition. Additionally, the FESEM images at low magnification (Figure S3A) for as-synthesized 82S sample show the flake-like particle collection and a similar result was obtained for 70S and 58S samples. These irregular flake-like shapes of all MBGs will be helpful for developing a polymer based bioactive glass composite scaffold for bone tissue engineering. Joseph and others reported that scaffold requires a comparatively better interaction between the filler particles and polymer matrix, which is accomplished well for the irregular shapes than the spherical ones [60]. Since, the large matrix is engaged in wetting particle surface in irregular shapes owing to their large surface area resulting in a good bonding between filler and polymer. In order to obtain more prominent information about the particle morphology of as-synthesized glass samples, HR-TEM technique is used. In Figure S4 (See ESI), we illustrate the HR-TEM image of pristine 58S sample where it retrieves the wormhole like mesoporous structure in disordered network.

3.5. In-vitro bioactivity test

The bioactivity test of all glass samples has been carried out through *in-vitro* study by the immersion of pristine samples in SBF solution for predetermined time intervals 1D, 3D, 5D and 7D (D: Days). The degradability or dissolution of mesoporous bioactive glass samples is analyzed by changing the pH of SBF solution with soaking time intervals due to ion-exchange process on the glass surface. Additionally, ICP-MS technique has been adopted for analyzing the ion-exchange kinetics during *in-vitro* test. Further, the prolonged soaking of samples has been analyzed by different analytical techniques to obtain correlation between the HCA formation and other physical properties discussed in the previous section.

3.5.1. Ion-exchange kinetics

In Fig. 6a, we illustrate the variation in pH value of SBF solution after immersing the as-prepared samples for different time intervals. Generally, pH of SBF solution increases rapidly with the immersion of samples in SBF due to strong ion-exchange process on the surface of glass sample with H^+ and H_3O^+ ions according to Hench Mechanism of HCA layer formation [61]. Here, the change in pH with time of soaking is increased marginally by 0.1 unit after one day, which shows weak ion-exchange of Ca^{2+} ions with hydronium ions. The dissolution of Ca^{2+} and PO_4^{3-} ions from the sample in SBF solution effectively depends on the chemical composition and textural parameters. The dissolution of ions increases with surface area but decreases with reduction in pore size [62]. In the present work, it is expected to have higher dissolutions of Ca^{2+} ions from the MBG due to high surface area with small pore size. However, we observe the smaller increment in pH value of SBF solution after immersion of MBGs suggesting that the size of pore effectively controls the ions dissolution from samples. Additionally, the dissolution of Ca^{2+} and PO_4^{3-} ions from the glass sample potentially affect the growth rate of HCA layer in SBF solution as the concentration of ions influence the precipitation of different phase of calcium phosphate (CaP) [63]. The minor increment in pH of SBF after one day immersion is not suitable for the formation and stabilization of HA/HCA layers on the surface of MBGs surface [64]. The chemical composition of bioactive glass also affects the bioactivity and all the three compositions have better bioactivity as per reported earlier [65]. The smaller pore size reduces the local increase of calcium and phosphorus ions in the SBF solution, as a result HCO_3^- and HPO_4^{2-} ions are dissociated as:



Typically, the percentage of H^+ ions in solution increases followed by a decrease in pH [64]. It has been reported that the increase of pH value by 2 units leads to 10-100 fold decrease of HCA solubility (stability increase), i.e., the substantial incremental value of pH leads to the apatite nucleation and stability of HCA layer [66]. Thus, the stability of CaP layer on the glass surface increases with pH value. It is known that a high pH environment is favorable for hydroxyapatite nucleation [67]. The rate of precipitation in the ionic solution simply defined as:

$$R_0 = kAS^n \quad (2)$$

where k = rate constant, A = area of contact of HA seeds, n = order of the reaction and S = the degree of supersaturation of solution which is defined as:

$$S = \left(\frac{IP}{K_{sp}} \right)^{\nu} \quad (3)$$

where IP = ionic activity product and K_{sp} = solubility product at equilibrium and value of K_{sp} of HA at 37 °C in aqueous solution is reported to be $10^{-17.2}$ and ν is the total number of ions that HA formed upon the solution (i.e., for $Ca_5(PO_4)_3OH$, $\nu = 9$) [68, 69]. The chemical reaction occurs in the formation of HA corresponds to $10Ca^{2+}$ and $6PO_4^{3-}$ ions per $2OH^-$ group (i.e., $10 Ca^{2+} + 6PO_4^{3-} + 2 OH^- = Ca_{10}(PO_4)_6(OH)_2$). Thus, the IP of HA is given by:

$$IP = \gamma(Ca^{2+})^{10} \gamma(PO_4^{3-})^6 \gamma(OH^-)^2 X [Ca^{2+}]^{10} [PO_4^{3-}]^6 [OH^-]^2 \quad (4)$$

where γ is the activity coefficient and $[OH^-] = K_w / [H^+] = K_w / 10^{-pH}$ in terms of pH value of solution, K_w = ion product constant for water. At physiological ionic strength, the value of $\gamma(Ca^{2+})$, $\gamma(PO_4^{3-})$ and $\gamma(OH^-)$ are 0.36, 0.06 and 0.72 respectively [70]. The change in IP of the apatite in SBF solution with time can be evaluated by substituting the activity coefficients, the element concentrations and pH values into Eq. 4. In Fig. 6b, we have shown the change in ionic activity product of apatite in SBF solution with soaking period for as-synthesized MBG samples. The calculation of IP confirmed the saturation of SBF solution after the immersion of MBG samples. All three samples have sufficiently large value of IP than reported in the literature [71]. According to the thermodynamic view, these as-synthesized MBGs possess the high potential for the formation of apatite.

Additionally, for the high rate of precipitation of ions in an ionic solution, the ionic activity product (simply defined as the concentration of ions in solution at present condition) should be higher as compared to the concentration of ions at equilibrium point (i.e., $IP > K_{sp}$). It has been

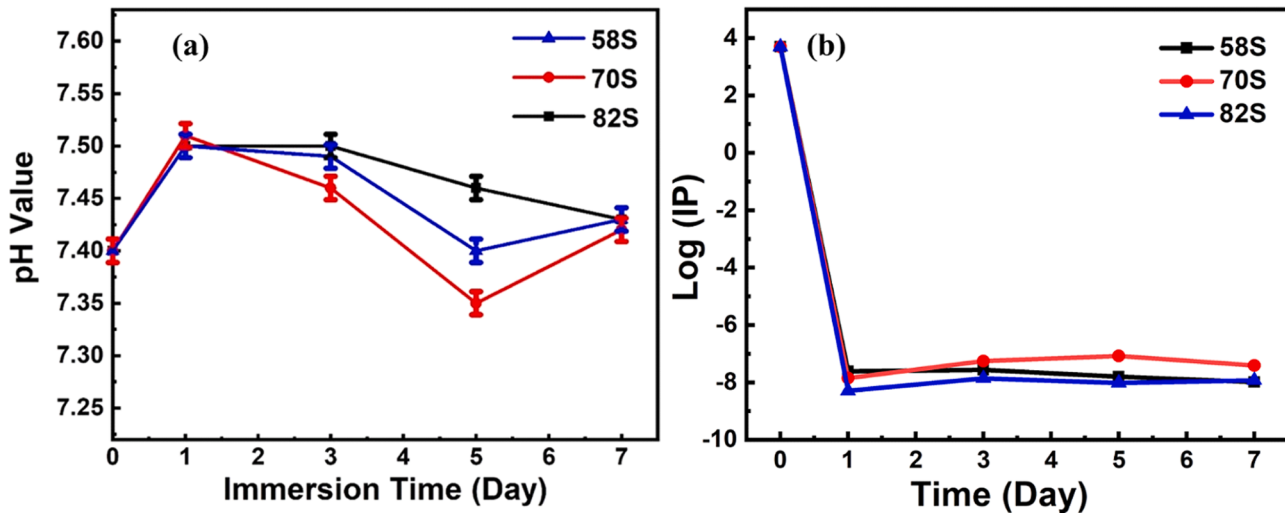


Fig. 6. (a) Change in pH value of SBF solution after the immersion of mesoporous bioactive glass samples with soaking time. (b) Change in ionic activity product (IP) of the apatite in SBF as a function of soaking time for 58S, 70S and 82S MBG samples.

reported that the nucleation rate is higher at the saturation condition of Ca^{2+} and PO_4^{3-} ions than normal concentration of the same ions. Thus, for biomimetic mineralization the concentration of calcium and phosphate ions must be higher than the concentration in saturation state. Additionally, the precipitation of CaP (stable or metastable phase) is sufficiently influenced by several factors such as degree of supersaturation (in SBF solution), the concentration of Ca^{2+} and PO_4^{3-} ions. The activation energy for CaP precipitation decreases with increase in the concentration of Ca^{2+} and PO_4^{3-} ions in physiological solution [63]. It has already been discussed that smaller pore size controls the dissolution of Ca^{2+} and PO_4^{3-} ions from the bioactive materials. Thus, the initial concentration of ions in SBF solution after the immersion of MBGs is not sufficient for the nucleation and crystallization of HCA for those MBG samples having high surface area and high density Si-OH group. As depicted in the FTIR results, as-synthesized MBGs stabilized through ethanol extraction process contained a high density of Si-OH group.

Additionally, it is worth noting that MBGs stabilized through the ethanol washing process are not completely free from the surfactant (P123), which is used as the structure-directing agent. The presence of P123 in the pore with a low amount also controls the dissolution of ions from the MBG samples. The high pH value of SBF solution during bioactivity test is favorable to the nucleation and crystallization of the HCA layer. However, in the present work the rise in pH value is not significant, hence, less nucleation and very poor or no crystallization of the HCA layer has been obtained. In general, the change in pH of SBF solution depends on different factors, e.g., textural parameters, buffering capacity of the surrounding solution, concentration of glass specimen in SBF solution and glass composition [37]. The pH and concentration of calcium and phosphate ions in the SBF solution during *in-vitro* bioactivity test effectively affect the rate of crystallization of HA/HCA on the surface of MBG samples. More prominently, to understand the biomineralization behavior of MBGs upon SBF soaking, we have undertaken the ICP-MS investigation.

3.5.2. ICP-MS analysis

ICP-MS technique has been adopted to monitor Ca and P elements concentrations in SBF solution after the immersion of as-synthesized MBGs for different time intervals of soaking, as shown in Fig. 7. It is evident that the concentration of Ca and P elements in SBF solution after 1 day of soaking sharply decreases, which indicate that high surface area with high silanol density directly follows the fourth stage of Hench Mechanism typically observed in MBGs. In contrast to conventional BG, the apatite formation on MBG surface in physiological solution doesn't

need to pass through first three stages of HM [72]. The slight increment in Ca^{2+} ions after three and five days reveals the less release of Ca^{2+} ions from MBGs and this behavior becomes more prominent in 58S glass than 70S and 82S, as 58S contain more Ca^{2+} ions on the surface confirmed by MAS-NMR results. Moreover, the decrement in concentration of Ca^{2+} ions in SBF physiological solution after five days of soaking ascribed by the formation of amorphous calcium phosphate layer over the silica-rich layer. The significant increment in P ions concentration in SBF solution after three days of soaking indicates the dissociation of HPO_4^{2-} ion into PO_4^{3-} and H^+ ions, as pH of SBF decreases for the same period. Furthermore, after five days of soaking, the reduction in phosphorous ion concentration indicates the formation of CaP clusters. In addition, it is also observed from ICP-MS data analysis as rapid decrement in Ca^{2+} ions in SBF solution reduces the driving force for ion-exchange reaction [66]. Here, the decrement in concentration of calcium ions after one day of soaking indicates the effective influence of textural properties and Si-OH group over the chemical composition. Different investigations have been carried out in such ternary system and reported by using the conventional sol-gel synthesis process. Among the various parameters, CaO content is the main factor for the formation and growth of HCA layer on the surface of conventional sol-gel synthesized glasses, while for the MBG textural parameters and silanol groups are more effective than chemical composition [9].

3.5.3. XRD study

In Figure S5 (See ESI), we illustrate the HR-XRD patterns for all SBF soaked samples after 7D (D: Days), where it reveals the amorphous nature of HA/HCA layer. The characteristic amorphous nature of HA/HCA layer is attributed to the combined effect of high surface area and high silanol density which leads to rapid degradation of active bioglass and less concentration of Ca^{2+} and PO_4^{3-} ions with respect to Si-OH group. We suggest that HA/HCA layer remains in amorphous phase due to small pore size of MBGs by which the CaP cluster's nucleation does not occur because smaller pore size limits the release of ions from MBGs. Along with these factors, ionic concentration of the physiological solution during *in-vitro* test also plays an essential role, which has already been discussed in the ion-exchange kinetics part. Consequently, the chemical constituents and textural properties of MBG sample affect the formation and growth of the HCA layer. The large surface area with high silanol density of MBG samples allows the large amount of SBF solution for *in-vitro* test which results in a considerable growth of HCA layer. The pH of SBF solution, ionic concentration, chemical constituents of the sample, Si-OH group density along with the textural parameters

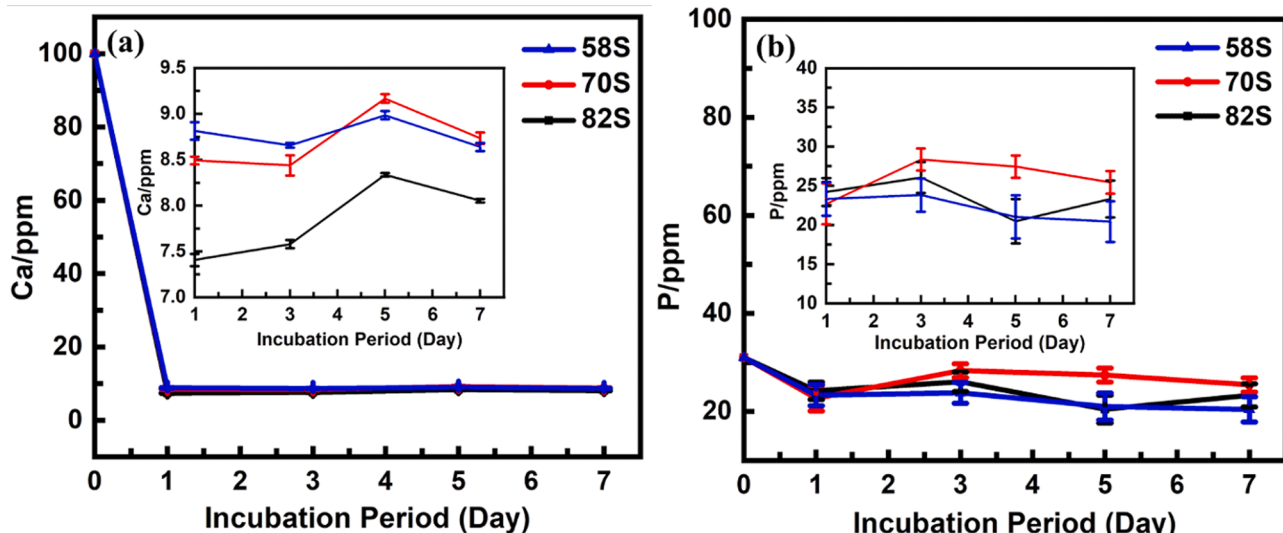


Fig. 7. (a) Ca and (b) P ions concentrations in SBF as a function of soaking time for 82S, 70S and 58S mesoporous bioactive glasses.

and composition of MBGs have an effective role in the formation of HCA layer during *in-vitro* bioactivity test.

3.5.4. FTIR spectroscopy study

The formation of HA/HCA layer on the surface of MBGs after *in-vitro* bioactivity test has been confirmed by FTIR spectroscopy study. In Figure S6 (See ESI), we illustrate FTIR spectrum of pristine and soaked samples after different time intervals. More evidently, the formation of HA/HCA layer upon soaking has been revealed by the corresponding characteristic bands. The broad vibrational band centered at 583 cm^{-1} corresponds to HCA phase and the intensity of this band increases with time of SBF soaking which confirms the formation of amorphous HCA layer. An appearance of the vibrational band at 1378 cm^{-1} corresponds to carbonate which evolves after seven days soaking of the 58S sample. The decrease in intensity of the vibrational band at 966 cm^{-1} reveals the information about ion-exchange and polymerization of SiO_2 . The band at 1635 cm^{-1} become less intense with time of soaking, which confirms the polymerization of Si-OH group on the surface of MBGs. The FTIR study on the SBF soaked samples confirms the formed HCA layer retained in amorphous phase in corroboration with the obtained HR-XRD results.

3.5.5. FESEM and HR-TEM analysis

FESEM and HR-TEM studies have been carried out to examine the morphological nature of SBF soaked samples. In Figure S7 (ESI), we illustrate FESEM micrographs of MBGs before and after soaking in physiological SBF for 3, 5 and 7 days. After three days of soaking, an uneven surface is obtained with the formation of HCA layer for all samples, which indicates the degradation of MBG samples in three days' time interval. The long-time period (seven days) for immersion of bioactive glass samples leads to the growth of HCA. The growth of HCA layer after five days of soaking is highest for the 70S samples than 82S and 58S samples as 70S sample possess greater surface area. It is known that the growth of HCA in case of sol-gel derived bioactive-glass mainly controlled by the textural properties [9]. The FESEM microscopy study directly provides information regarding the degradation of mesoporous bioactive glasses by the change in the surface morphology with soaking time intervals. Hence, the growth of amorphous HCA layer on the surface of immersed sample is enhanced with the surface area. In Figure S8, we show the HR-TEM micrograph in bright field mode reveals significant changes on the glass structure with SBF soaking period. The HR-TEM image of SBF soaked 58S sample after three days of soaking

gets modified into a random array of pores with the incorporation of amorphous CaP. After seven days of soaking interval, a flaky like layer of amorphous HCA has been observed.

3.5.6. MTT Assay

The cytotoxicity analysis of MBG samples at different concentrations of 10, 20, 50 and $100\text{ }\mu\text{g ml}^{-1}$ are performed and calculated using MTT assay after an interaction time of 24, 48 and 72 hrs. In this study, the U2OS human osteosarcoma cells are cultured in DMEM-F12 and untreated cells are taken as 100 percent viable. The cellular viability of all three MBG samples with different concentration ratio and interaction time are measured. In Fig. 8a, we illustrate the viability of human U2OS cells on treatment with different concentrations of 58S, 70S and 82S MBG samples after culturing for 24 hrs. The data clearly shows a significant difference amongst the samples in this concentration range of MBGs. We observed high cellular viability of 58S MBG at all concentrations for 24 hrs. In contrast to the 58S MBG sample, the 70S and 82S MBGs at 10 and $20\text{ }\mu\text{g ml}^{-1}$ concentration show better biocompatibility, whereas higher concentrations of 50 and $100\text{ }\mu\text{g ml}^{-1}$ appears to exhibit lower cell viability. Thus, the increase in concentration, especially after $> 20\text{ }\mu\text{g ml}^{-1}$ all MBG samples demonstrate lowering of cell viability. Such significant disparity in cell viability of MBGs samples (only for 24 hrs. interaction time) with different concentrations strongly depends on the soluble ions such as Si, Ca and P ions. Moreover the degradation of MBGs are effectively controlled by the pore architectures such as pore size and surface area. For the 58S MBG sample, we have a larger pore size than 70S and 82S, from the ICP-MS results, the dissolution of ions for 58S is higher than 82S and significantly less for 70S due to its small pore size. The dissolution of Si, Ca and P ions from the MBGs is crucial for accelerating osteogenesis by regulating osteoblast proliferation, differentiation and gene expression [73,74]. In Fig. 8b, we illustrate the cellular viability of 58S, 70S and 82S MBG samples at $10\text{ }\mu\text{g ml}^{-1}$ concentrations with varying interaction time. Here, we observed that the cell viability remains more than 80 % for all MBG samples even after 72 hrs of the treatment and highest for 58S MBG sample than the other two samples. Thus, the cell viability and cytotoxicity of as-synthesized MBGs strongly depends on the pore architecture, therefore it is necessary to investigate the appropriate concentrations of as-prepared samples for the acceleration of osteogenesis process. More specifically, both P and Ca ions play vital role in promoting the bioactivity and formation of a mineralized extracellular matrix. In addition, Si ions are also important for accelerating the osteoblast growth. It is observed that the MBGs

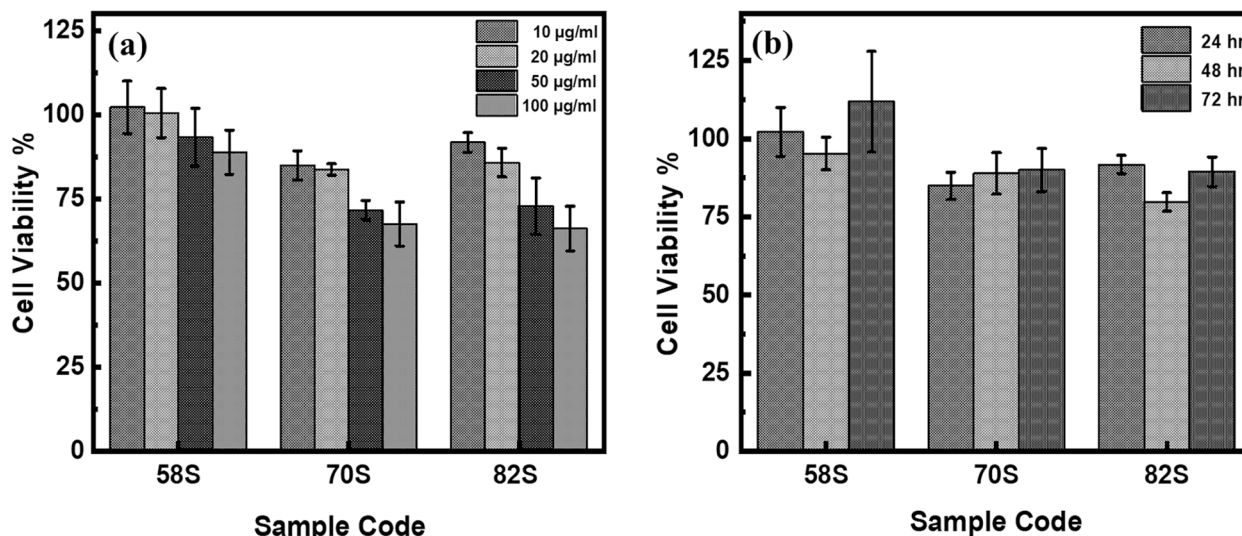


Fig. 8. (a) Human osteoblast-like osteosarcoma cell (U2OS) attachment viability on 58S, 70S and 82S MBG samples with different concentrations levels after culturing for 24 hr. (b) Human osteoblast-like osteosarcoma cell (U2OS) attachment viability on 58S, 70S and 82S MBG samples for different time intervals.

- [59] K. Lukowicz, B. Zagrajczuk, A. Nowak, L. Niedzwiedzki, M. Laczka, K. Cholewa-Kowalska, A.M. Oszyczka, *Mater. Sci. Eng. C* 109 (2020), 110535.
- [60] R. Joseph, W.J. McGregor, M.T. Martyn, K.E. Tanner, P.D. Coates, *Biomaterials* 23 (2002) 4295–4302.
- [61] L.L. Hench, *J. Am. Ceram. Soc.* 81 (1998) 1705–1728.
- [62] Yu-Jen Chou, Bo-Jiang Hong, Ying-Chih Lin, Chen-Ying Wang, Shao-Ju Shih, *Materials* 10 (2017) 488.
- [63] X. Lu, Y. Leng, *Biomaterials* 26 (2005) 1097–1108.
- [64] S. Jebahi, H. Qudadesse, E. Wers, J. Elleuch, H. Elfekih, H. Keskes, X.V. Bui, A. Elfeki, *World Acad. Sci. Eng. Technol. Int. J. Mater. Metall. Eng.* 7 (2013) 304–309.
- [65] M.M. Pereira, A.E. Clark, L.L. Hench, *J. Biomed. Mater. Res.* 28 (1994) 693–698.
- [66] M. Bohner, J. Lemaitre, *Biomaterials* 30 (2009) 2175–2179.
- [67] W.P. Inskeep, J.C. Silvertooth, *Geochim. Cosmochim. Acta* 52 (1988) 1883–1893.
- [68] E.C. Moreno, K. Varughese, *J. Cryst. Growth* 53 (1981) 20–30.
- [69] S.V. Dorozhkin, M. Epple, *Chem.-Int Ed* 41 (2002) 3130–3146.
- [70] C. Ohtsuki, T. Kokubo, T. Yamamoto, *J. Non-Cryst. Solids* 143 (1992) 84–92.
- [71] X. Yan, X. Huang, C. Yu, H. Deng, Y. Wang, Z. Zhang, S. Qiao, G. Lu, D. Zhao, *Biomaterials* 27 (2006) 3396–3403.
- [72] P.N. Gunawidjaja, A.Y.H. Lo, I. Izquierdo-Barba, A. Garcia, D. Arcos, B. Stevensoon, J. Grins, M. Vallet-Regí, M. Edén, *J. Phys. Chem. C* 114 (2010) 9345–19356.
- [73] P. Saravanapavan, J. Selvakumaran, L.L. Hench, *Key Eng. Mater.* 254 (2004) 785–788.
- [74] C. Wu, R. Miron, A. Sculean, S. Kaskel, T. Doert, R. Schulze, Y. Zhang, *Biomaterials* 32 (29) (2011) 7068–7078.
- [75] H.S. Yun, J.W. Park, S.H. Kim, Y.J. Kim, J.H. Jang, *Acta Biomater* 7 (2001) 2651–2660.
- [76] B. Li, X. Chen, B. Guo, X. Wang, H. Fan, X. Zhang, *Acta Biomater* 5 (2009) 134–143.